ISSN 2070-2051, Protection of Metals and Physical Chemistry of Surfaces, 2016, Vol. 52, No. 5, pp. 859–868. © Pleiades Publishing, Ltd., 2016.

NANOSCALE AND NANOSTRUCTURED MATERIALS AND COATINGS

Growth, Corrosion and Wear Resistance of SiC Nanoparticles Embedded MAO Coatings on AZ31B Magnesium Alloy[1]

Hadi Nasiri Vatan, Reza Ebrahimi Kahrizsangi*, and Masoud Kasiri Asgarani

Advanced Materials Research Center, Materials Engineering Department, Najafabad Branch, Islamic Azad University, Najafabad, Isfahan, Iran

**e-mail: rezaebrahimi@iaun.ac.ir*

Received May 28, 2015

Abstract—In this research, nanocomposite coating was deposited on magnesium matrix AZ31B alloy using the micro arc oxidation (MAO) method. MAO was carried out in SiC-nanoparticles containing suspension using the sodium silicate and sodium aluminate bases at constant current density. The effect of nanopowder addition and MAO periods were also investigated in the present work. Using the Scanning electron microscopy (SEM), the thickness and surface morphology of the coatings were studied. The coefficient of friction and abrasion rate curves were used to analyze nanopowder addition on resistance to abrasion, while the potentiodynamic curves were used for assessing the resistance to corrosion in the ceramic nanocomposite coating deposited on surface of alloy AZ31B. The morphological studies on surface of coatings revealed that the cavitation level and size increases with the increasing coating duration. Besides, Energy Dispersive X-Ray Diffraction (EDS) analyses from cross section and surface of the prepared coatings revealed that nanopowder distribution on interface of coating with matrix and boundaries of the cavities is almost uniform. The cross section studies of the coatings revealed that their thickness increases, as coating duration prolongs. Furthermore, the corrosion behavior of the samples indicated that presence of nanopowder does not significantly affect the resistance to corrosion of the coatings; however, coefficient of friction and abrasion rate of coatings indicates a respective rise and drop in presence of these nanopowders.

DOI: 10.1134/S2070205116050257

INTRODUCTION

Magnesium and its alloys have a generally low resistance to corrosion. This shortcoming has limited non-coated application of magnesium alloys in the corrosive media. Since magnesium and its alloys are highly liable to galvanic corrosion, resulting in their decreased mechanical stability and creating an undesired appearance, surface treatments are required for improving their surfaces [1]. By now, various coating methods have been studied for protection of magnesium and its alloys against the corrosion. Among these methods are electrochemical plating, gas phase deposition, conversational coatings, anodizing, laser surface alloying, and polymer coatings.

Nanocomposites are among the most common coatings for surface protection against the corrosion, as they involve excellent properties such as resistance to corrosion and abrasion, ductility, etc. [2, 3]. Recently, MAO method has been applied for preparation of these coatings. Anodizing is the most common technique among the conversion coatings method, as it is relatively simple and inexpensive. However, the coatings prepared using this method have low thickness and high porosity, so that they cannot provide the required resistance to corrosion in the corrosive media. MAO is a relatively new preferential surface treatment method for protection against the corrosion of magnesium and its alloys [4]. The method is on basis of the anodic polarization of a metal or alloy in electrolyte [1]. The main difference between MAO and anodizing is in the applying voltages higher than that of oxide layer breakdown [5], leading to the local generation of sparks with gas release [1]. As a result, sample surface is converted to a relatively thick and hard ceramic oxide coating through the sparking process. Many works show that the phase/chemical composition and corrosion behavior of coatings deposited on magnesium and its alloys are basically controlled by process parameters, and chemical composition of the materials and electrolyte. Furthermore [1, 5–7], a large number of works show that breakdown voltage is among the most important parameters controlling the properties of the developed coating [1].

SiC is used for synthesis of nanocomposite layers using techniques including electroplating, arc-discharge plasma, gas flume spray, vacuum deposition methods, high temperature glass annealing, laser surface modification, and thermal spray. However, it

[1] The article is published in the original.

Table 1. Relative composition of magnesium AZ31B alloy determined using the quantometer analysis

Element	Mg	Zn	Si	Mn	Fe	Cu	Al
wt %	95.603	1.017	0.022	0.312	0.003	0.036	3.007

must be noted that these methods need high substrate temperature for creation of sufficient cohesion against the developed high contact loads [2, 8, 9]. Nanoparticles such as alumina and zirconia are used for preparation of nanocomposite coatings on substrates such as aluminum and titanium using the MAO method for enhancing resistance to corrosion, resistance to abrasion, thermal properties, mechanical strength, and coating cohesion to matrix. In this regard, the practical research works are mainly focused on aluminum and its alloy, rather than magnesium and its alloys [10–12]. Thus, applying the MAO and using electrolyte containing SiC nanopowder and study of coating duration at constant current density on magnesium matrix AZ31B alloy, in this work an attempt was made to prepare a relatively thick ceramic. The resistance to corrosion and resistance to abrasion of this coating are enhanced because of the prepared ceramic coating and addition of nanopowders to the coating, respectively.

EXPERIMENTAL PROCEDURE

The samples used in this work are made of magnesium AZ31B alloy prepared as plates with thickness of 20 mm. The relative composition of this alloy obtained by quantum analysis is shown in Table 1.

To carry out the experiments, rectangular cubic samples were prepared using the purchased plate. Preparation of samples included sanding using the SiC paper sands via five steps including meshes 200, 800, 1200, 2500, and 4000. DI water and hot air current were used for sample washing and drying, respectively. To attach samples to the holder (which plays the role of anode in the electroplating system), the samples were drilled and screw threaded from their smaller surface.

The composition of electrolyte used in MAO process is 2 g/L $NaAlO_2$, 2 g/L Na_2O_3Si, 0.5 g/L KOH (all Merck), and 5 g/L SiC nanoparticles with a size lower than 80 nm (Figs. 1, 2). SEM apparatus (Philips CM120, Netherland) was utilized to determine size of SiC nanoparticles. To weight chemicals and samples, the accurate scale model A&D-GR202 with precision $\pm$ 50 μg was used. For a more unified distribution of nanoparticles, the suspension was stirred for 6 h using a stirrer.

The system applied for MAO process consists of a 20 kW electrical power source, current rectifier with maximum output voltage of 600 V, and an electrolyte cooling system maintaining electrolyte temperature at 30°C. During the coating process, the density of the applied current was 23.1 mA/cm^2 and coating durations were 5, 10, 15, and 20 min. Once the coating process was completed, the samples were extracted from electrolyte, washed with DI, and dried with hot air current (Table 2).

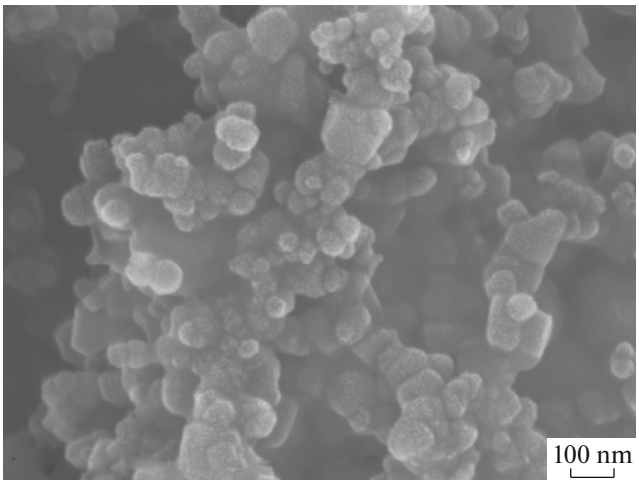

Fig. 1. SEM image of used SiC nanopowder.

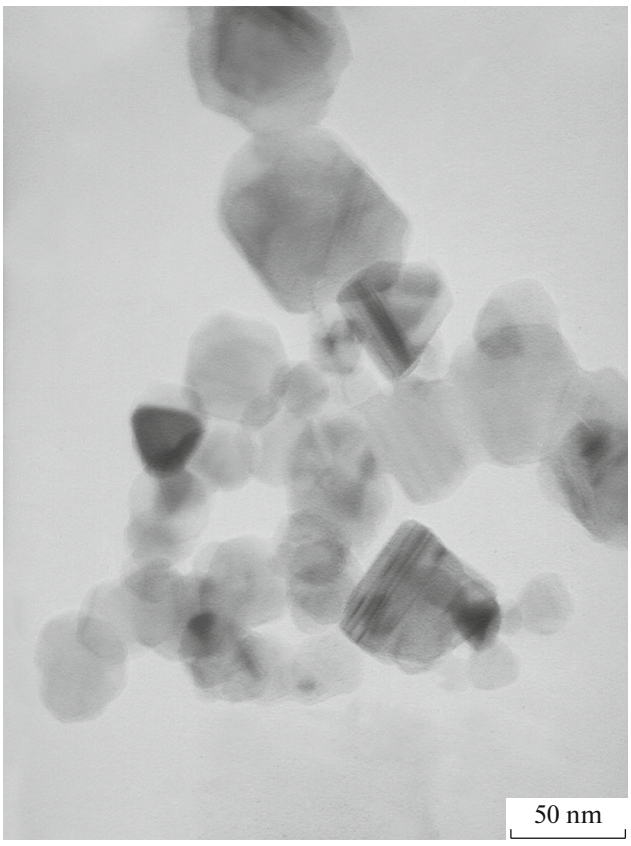

Fig. 2. TEM image of used SiC nanopowder.

To study the surface morphology, cross section, and composition of the prepared coatings SEM devices (TESCAN, Ztech), VEGA equipped with EDS analysis probe (ROTEC), and ZEISS (SIGMA/VP, Germany) were used. Before cross sectional analysis of the samples, they were grooved using the fretsaw, mounted using the special resin, sanded, and polished. To study SEM images and calculation of porosity level, pore size, and coating thickness, image analyzer software ImageJ was used. The potentiodynamic polarization tests were conducted using the potentiostat/galvanostat apparatus (EG&G, 273). To enhance accuracy of the experiments and equalization of test conditions for all samples, the experiments were performed in the three-electrode standard flatcell of the system.

In this model, the sample, platinum net, and saturated potassium chloride calomel electrode (SCE) were used as the working electrode (WE), auxiliary electrode (AE), and reference electrode, respectively. The electrolyte used for the corrosion tests were a solution with 3.5 wt % NaCl, while the interfacial area of electrolyte and samples were 0.196 cm^2. Before the corrosion tests, samples were dipped into the solution for 30 min, so that their potential reaches an almost constant level. All corrosion tests were conducted at ambient temperature. The potential range applied for these experiments varies from −300 mV (vs. OCP) to +700 mV (vs. OCP), with scanning rate of 1 mV/S. To analyze the obtained results, SoftcorrIII software was applied. Here, the PARCalC analysis of the software was utilized for analysis of potentiodynamic polarization curves, with respect to their anodic and cathodic regions. The surface roughness (R_a) of the prepared coatings was measured using the Stylus type Surface Profilometer (Taylor Hobson Sutronic-25) with precision of ± 10 nm. The experiment was carried out three times for each sample and the result was reported as their mean value. To study resistance to abrasion and coefficient of friction of coatings, Pin-on-Disk abrasion test was conducted according to the ASTM G-99 standard. To determine thickness of the prepared samples, thickness gauge device (QniX-8500) were used. The thickness measurements were carried out 18 times and the output was reported as their mean value.

RESULTS AND DISCUSSION

Figure 3 illustrates potential variations with time for samples coated for 20 min. For shorter durations, the coated samples indicate higher correlation with these curves. So, because of the high similarity, only samples coated at longest duration without nanopowder were reported. The obtained results are similar to those reported to the similar works, as it is shown that the sample coated in suspension containing nanopowder indicates 10–15 V sparking potential less than that of sample without nanopowder [13]. At the beginning of sparking process, layer resistance is not considerably high, so that to maintain the current a higher voltage rise is required. After 100 s, coating resistance reaches a constant amount, exceeding which voltage rise rate is constant. The results show that resistance of nanocomposite coating is slightly smaller than that of coating without nanopowder.

Table 2. Durations applied for MAO process

Sample code	Nanopowder	Time of coating, min
NP5	SiC	5
NP10	SiC	10
NP15	SiC	15
NP20	SiC	20
SS5	–	5
SS10	–	10
SS15	–	15
SS20	–	20

Figure 4 presents SEM images from free surface of the prepared coatings. As shown in the figure, the time increase results in the corresponding increase in mean pore size. Table 3 shows the weight, thickness, and mean pore size of the obtained coatings. The table also shows that samples containing nanopowder are denser than those without nanopowder. This finding is consistent with the similar cases reported for nanocomposite preparation using the PEO method [14, 15].

Moreover, Fig. 5 illustrates the images and element distribution at surface of nanopowder-containing coatings. The figure shows that all elements have a rather similar distribution in the coatings.

In Table 3, the difference between initial and final weight of the coated samples is shown, where all differences are positive, implying the further growth of

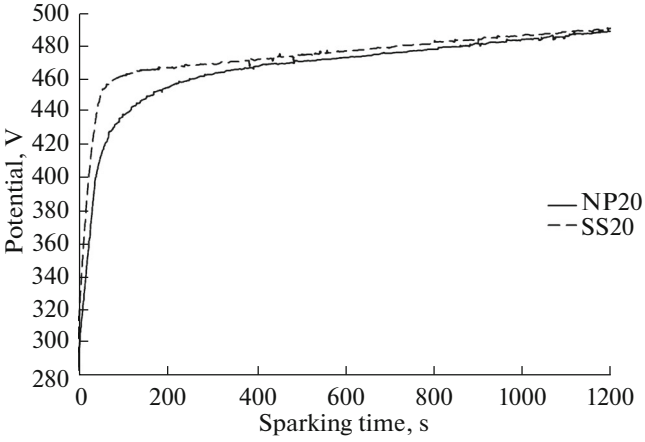

Fig. 3. Potential variation with time for samples coated for 20 min.

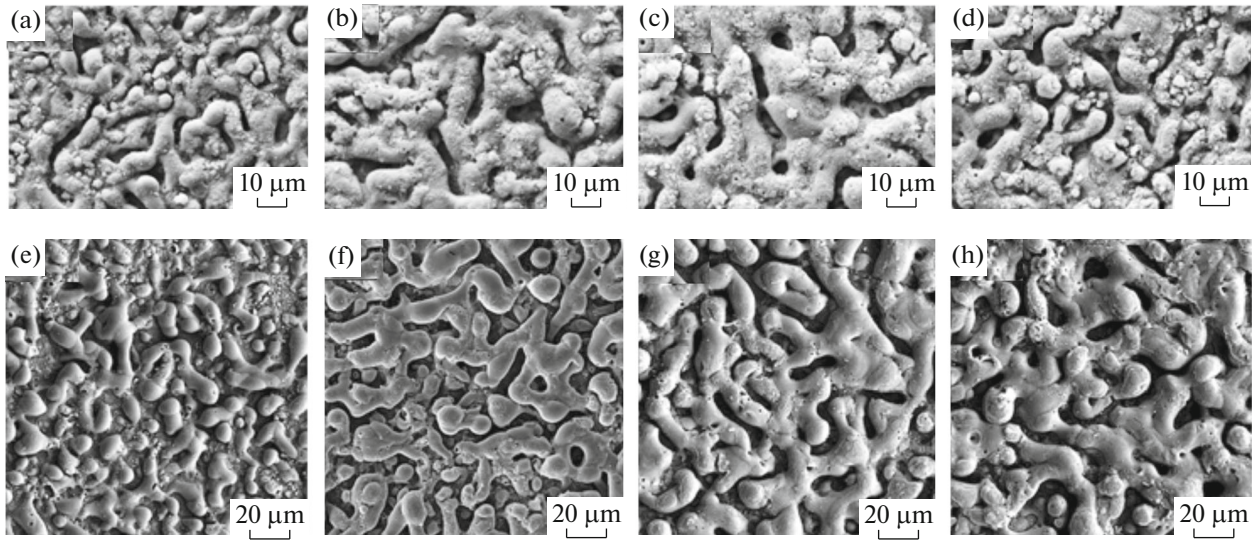

Fig. 4. SEM image from free surface of the prepared coatings including: (a) NP5; (b) NP10; (c) NP15; (d) NP20; (e) SS5; (f) SS10; (g) SS15; and (h) SS20.

coating as compared to the matrix consumption. Moreover, as expected, weight difference increases as time proceeds. Further examination of the specimens with profilometer indicates that both coating thickness obtained from the probe and porosity rise by time. According to the previous studies, the increase in coating time and addition of nanoparticles result in the increased porosity and cavity blockage, respectively. For a more elaborate study, SEM images from cross section of coatings are shown in Fig. 6. The mean thickness estimated using these images (shown in Table 3) indicates a further increase in coating thickness with time. Besides, due to the rough surface and porosity of the coatings, the coating thickness measured from cross section SEM images is 2.5–3.5 times greater than the one measured by the probe.

Table 4 presents the EDS results for free surface of the prepared coatings. The results indicate that as time proceeds, aluminum percentage is more or less constant for specimens with nanopowder. However, time increase in these specimens results in the increased nanopowder absorption. It is observed that as coating time prolongs a respective increase and decrease is observed in silicon and magnesium weight percentages. The increased nanoparticle content of specimens can be probably attributed to the reduced magnesium oxide phase. In this research, the maximum silicon introduction to the coating was 27% (sample NP20).

Table 3. Weight, thickness, and mean pore size of the prepared coatings

Sample code	Weight before PEO, g	Weight after PEO, g	Weight difference, mg	Average of hole diameter, μm	Probe thickness, μm	Porosity percent	Cross thickness, μm	$\frac{\text{Probe thickness}}{\text{Cross thickness}}$
NP5	5.0818	5.08805	8	5.95	11.42	15.47	4.15	2.75
NP10	5.24286	5.25608	13	7.83	13.65	17.17	4.67	2.92
NP15	5.23899	5.25909	20	8.31	17.57	18.21	5.97	2.94
NP20	5.13530	5.16194	27	8.56	33.56	19.45	13.06	2.57
SS5	5.22239	5.22879	6	6.32	12.99	15.55	4.06	3.20
SS10	3.55180	3.56295	11	8.12	15.99	18.17	4.48	3.57
SS15	5.10653	5.13181	25	9.27	16.79	19.29	4.81	3.49
SS20	5.12214	5.15236	30	10.22	32.99	22.17	12.99	2.54

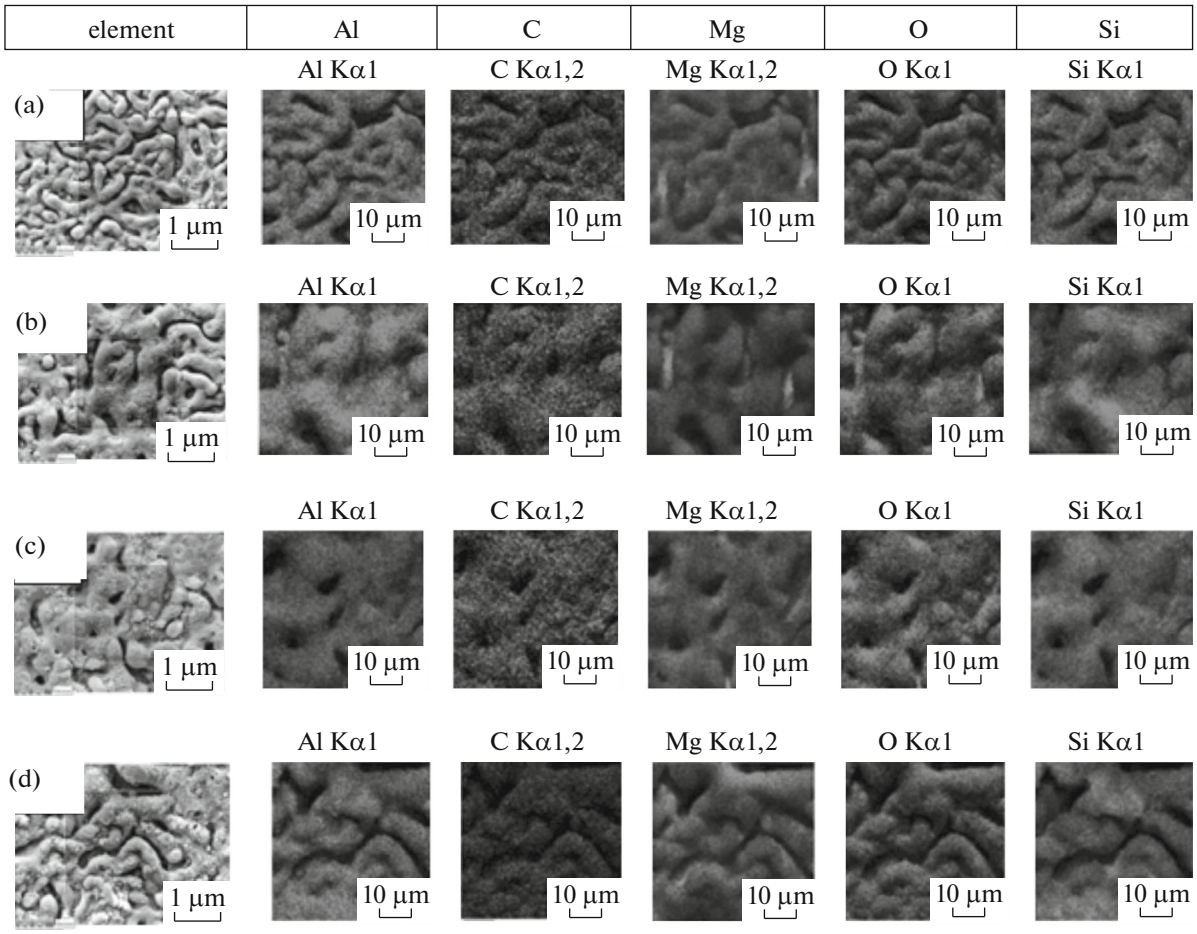

Fig. 5. Distribution map of elements inside the developed coatings including: (a) NP5; (b) NP10; (c) NP15; and (d) NP20.

Figure 7 presents the element distribution inside the coatings. As shown in the figure, elements have a uniform distribution inside all coatings. This is even true for silicon distribution in samples with nanopowder. However, it was also observed that for some samples the oxygen loss induced by presence of nanopowder is slight near the exterior surface of the coating is less, while silicon distribution is stronger and more unified inside the coating and toward the coating/matrix interface.

Figure 8 illustrates a cavity developed in sample NP15, coated with SiC. It seems that nanoparticle absorption inside occurs inside the cavities and, majorly, at their ends, while a smaller share of nanoparticles are absorbed on their walls.

Figure 9 shows the curves extracted from potentiodynamic polarization of the coatings. As indicated by the figure, the behavior of samples without nanopowder and nanocomposite samples is rather similar, and no significant difference is observed in cathodic and anodic slopes and the behavior of anodic branch, except the current density and corrosion rate drop in presence of nanoparticles which is attributed to the cavities blockage. However, this factor does not lead to

Table 4. EDS results obtained from free surface of the obtained coatings

Sample code	C, wt %	Si, wt %	O, wt %	Mg, wt %	Al, wt %
NP5	16.3	13.4	22.6	34.4	13.3
NP10	17.5	23.7	19.8	25.8	13.2
NP15	16.9	26.1	21.1	22.8	13.1
NP20	15.1	26.9	20.6	24.1	13.3

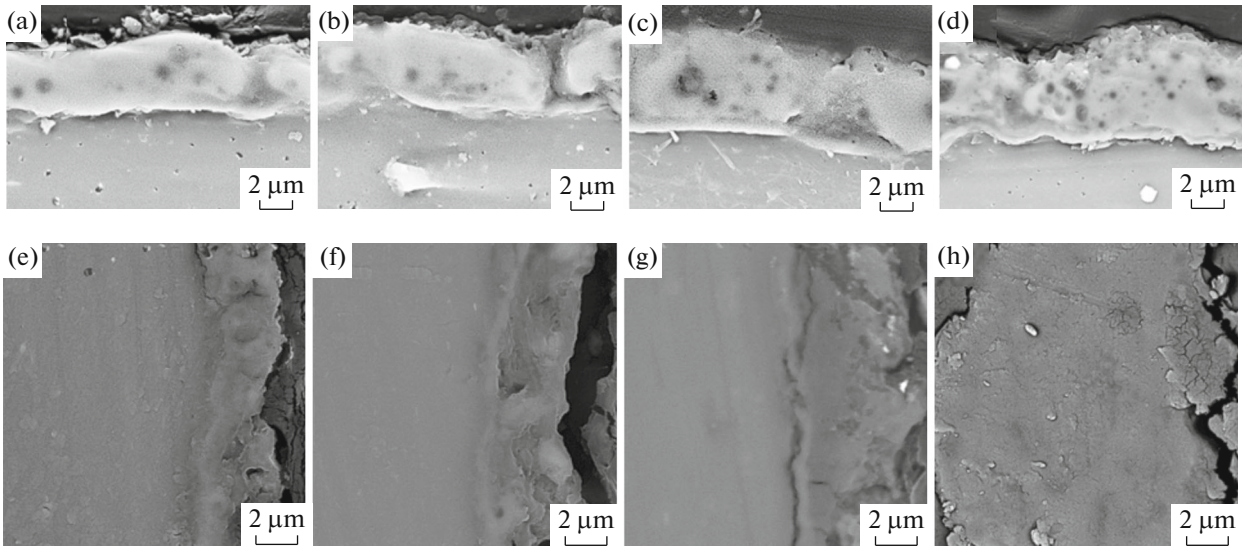

Fig. 6. SEM images from cross section of the prepared coatings including: (a) NP5; (b) NP10; (c) NP15; (d) NP20; (e) SS5; (f) SS10; (g) SS15; and (h) SS20.

a considerable drop in current density and corrosion rate [16, 17].

The results extracted from Fig. 9 are summarized in Table 5. As shown in the table, samples containing nanopowder are slightly shifted toward the more active values, indicating their higher tendency to corrosion [18–20].

The sharp passive layer breakdown for samples without nanoparticle is only observed for coating time of 20 min. Indeed, the passive region indicates a sharper breakdown as compared to the rest of coating times. On the other hand, for samples with nanopowder, except NP5, passive layer does not show a distinct failure. Thus, it can be stated that presence of nanopowder facilitates development of passive region [21].

Figure 10 shows abrasion curves for samples with and without nanopowder. Also, Fig. 11 illustrates the SEM images from abrasion surface of the prepared coatings, while Table 6 summarizes their abrasion rate, abrasion groove width, roughness, and hardness data. A relatively similar trend was observed for samples without nanopowder, except sample SS10 which indicates a lower coefficient of friction with is almost constant even after addition of nanopowder; however, corrosion rate and groove width indicate a significant drop after nanopowder addition [22, 23].

Probably, the material of coating with and without nanopowder does not indicate a considerable phase difference, unless in presence of nanopowder the strength and corrosion rate of the coatings indicate a respective rise and drop [24, 25]. Moreover, coating

Table 5. Results extracted from Fig. 9

Sample code	$\beta_a \times 10^{-3}$, V/decade	$\beta_c \times 10^{-3}$, V/decade	R_p, kOhm s/cm^2	E_{corr}, V vs. SCE	C.R, mpy	i_{corr}, μA/cm^2	E_b, V	Passive Region ($E_b - E_{Corr}$), mV
NP5	86.48	149.9	1.30	1.501	16.58	18.38	−1.47	31
NP10	359.8	156.5	2.23	−1.486	19.15	21.23	−1.4	86
NP15	120.5	228.3	2.97	−1.472	10.39	11.52	−1.39	82
NP20	111.5	157.6	3.08	−1.489	8.30	9.20	−1.39	99
SS5	69.14	320.8	0.24	−1.505	92.55	102.60	−1.47	35
SS10	122.2	167.4	1.53	−1.427	18.11	20.08	−1.4	27
SS15	67.54	200	0.59	−1.462	33.65	37.31	−1.41	52
SS20	188.2	223.2	1.39	−1.460	28.73	31.85	−1.35	110

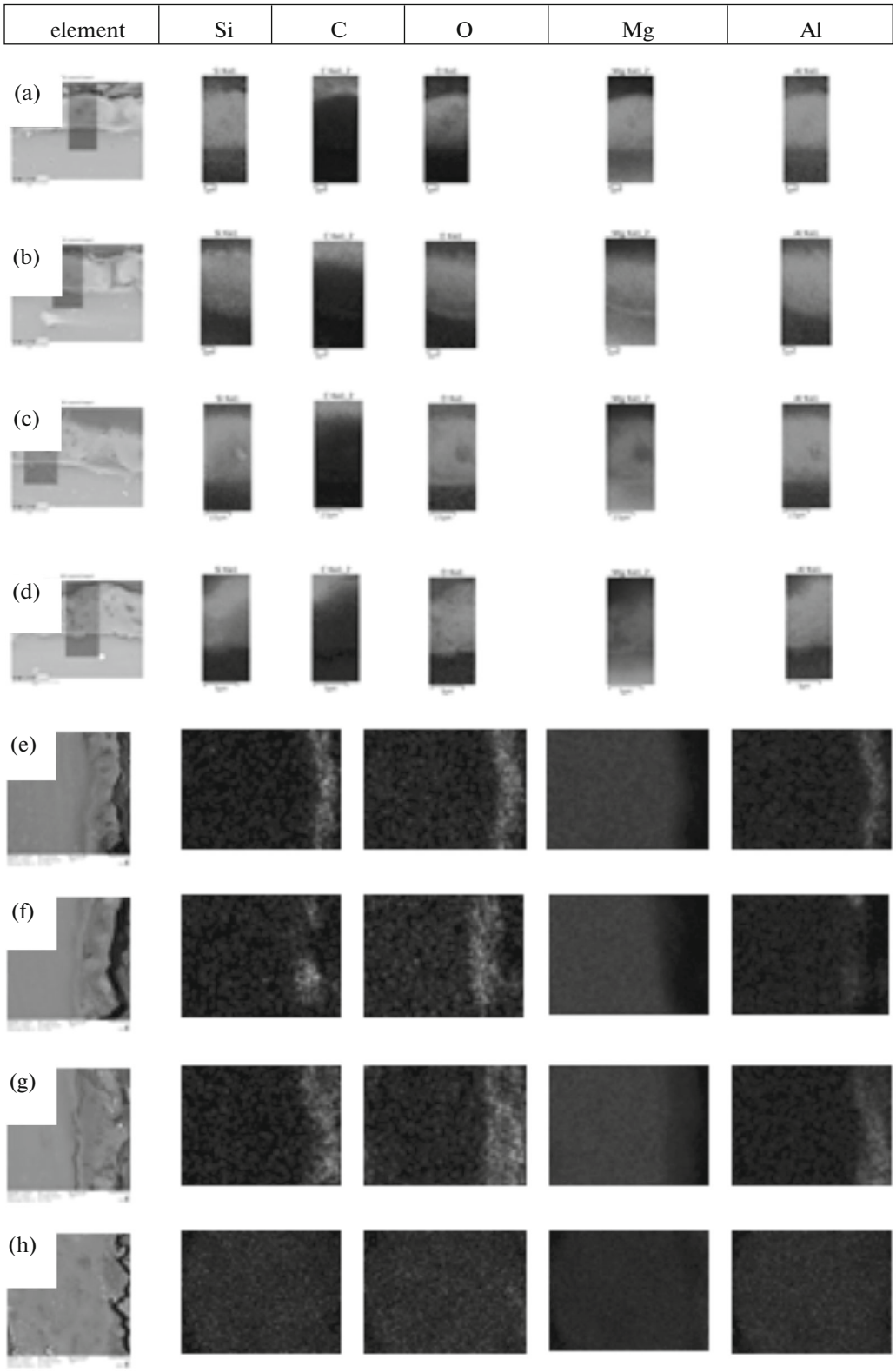

Fig. 7. Distribution map of elements inside the prepared coatings: (a) NP5; (b) NP10; (c) NP15; (d) NP20; (e) SS5; (f) SS10; (g) SS15; and (h) SS20.

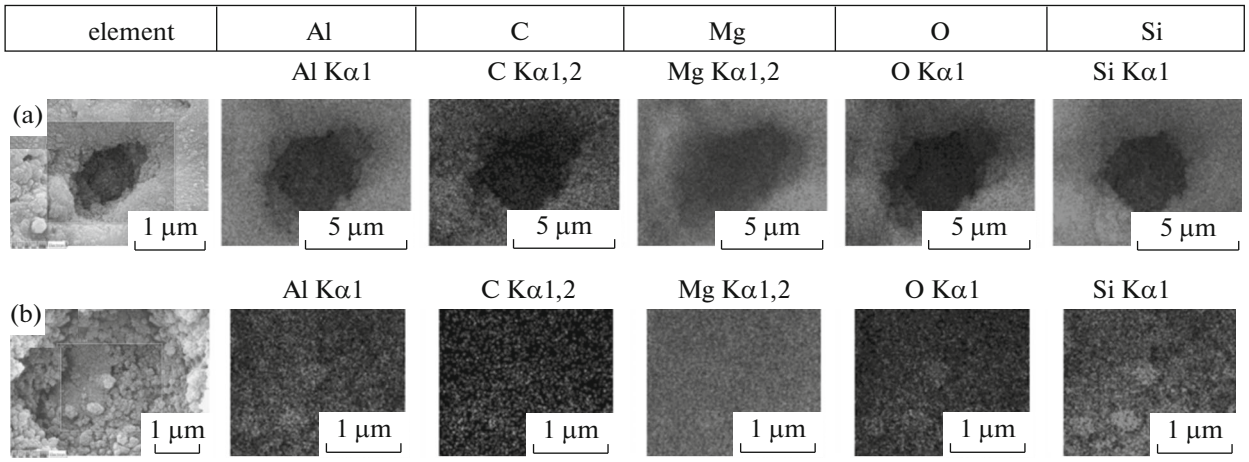

Fig. 8. Representation of a cavity in sample NP15 coated with SiC: (a) outside of the pore; and (b) pore floor.

roughness indicates a slight drop by addition of nanopowder, which does not have a noticeable impact on abrasion results [26, 27]. The results show that addition of nanopowder results in a drop in abrasion rate from 24×10^4 to 13 (mg/m N) $\times 10^4$.

Based on the obtained results, it seems that samples NP10 and NP15 are the best in terms of corrosion and abrasion behaviors, as they also have an average coating duration in presence of nanoparticles.

CONCLUSION

In this work, effect of coating time and presence of SiC was studied on PEO nanocomposite coating. The sample coated in suspension containing nanopowder indicated a 10–15 V lower sparking potential as compared to the samples without nanopowder. The increase in coating time resulted in a rise in mean pore

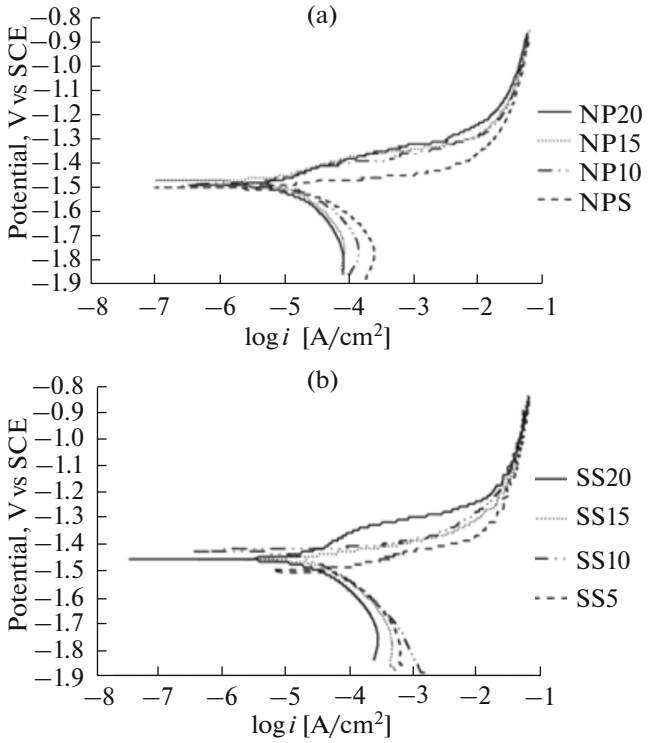

Fig. 9. Potentiodynamic polarization curves for samples: (a) with nanopowder; and (b) without nanopowder.

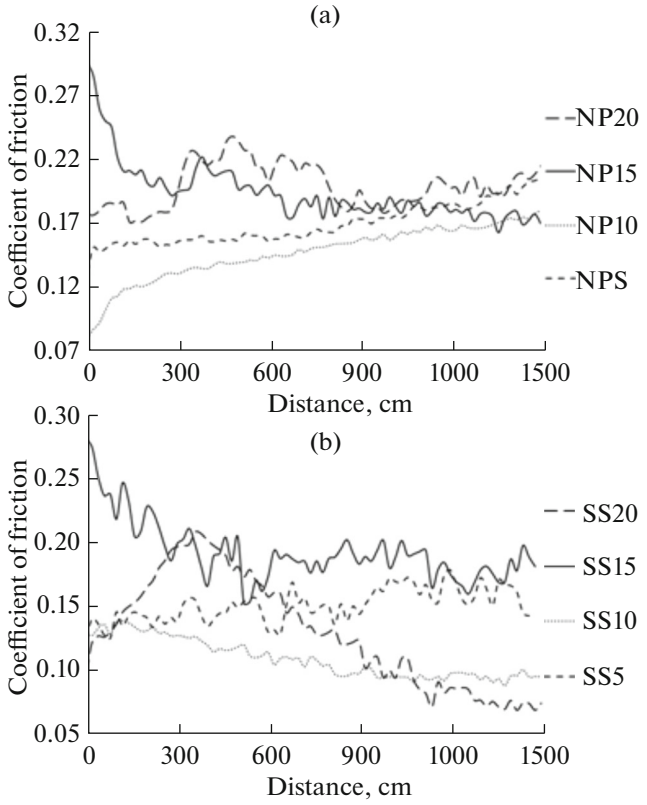

Fig. 10. Coefficient of friction curves for: (a) samples with nanopowder; and (b) samples without nanopowder.

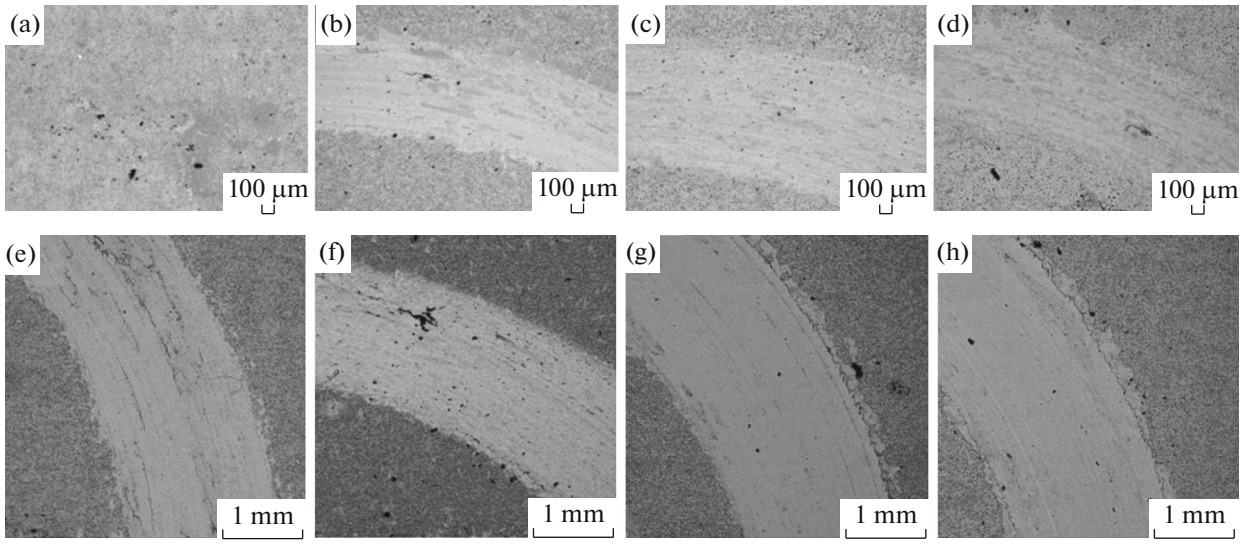

Fig. 11. SEM image from abrasion surface of the prepared coatings: (a) NP5; (b) NP10; (c) NP15; (d) NP20; (e) SS5; (f) SS10; (g) SS15; and (h) SS20.

size from 5.95 to 8.56 μm for samples with nanopowder and 6.32 to 10.22 μm for samples without nanopowder, the varying weight difference of 0.008–0.027 mg for sample with nanopowder and 0.006–0.03 mg for samples without nanopowder, porosity level from 15.47–19.45% for samples with nanopowder and 15.55–22.17% for samples without nanopowder, and coating thickness 4.15–13.06 μm for samples with nanopowder and 4.06–12.99 μm for samples without nanopowder. Furthermore, samples with nanopowder were found to be denser as compared to those without nanopowder. As time proceeds, the element distribution is more or less constant in samples without nanopowder, while it increases from 13.4 to 26.9% for samples containing nanopowder. Element distribution is almost the same inside all specimens. Nanoparticle absorption occurs inside the cavities and mainly in the cavity ends, while the wall indicated low nanoparticle absorption. The corrosion behavior of the samples without nanopowder and nanocomposite samples is relatively similar, where the anodic and cathodic slopes and the behavior of the anodic branch does not indicate a significant difference. Presence of nanopowder facilitates development of the passive zone. Different layer breakdown and abrasion behavior was not observed for any sample. By addition of nanopowder, the mean coefficient of friction indicated no considerable difference; however, the mean abrasion rate indicated a drop from 24×10^4 to 13 (mg/m N) $\times 10^4$ and width of abrasion groove was decreased from 1.888 to 1.003 μm.

Table 6. The groove width, abrasion rate, roughness, and hardness data of the coatings

Sample code	Average of Friction Coefficient	Wear Track Width, μm	Wear Rate, mg/(m N) $\times 10^{-4}$	Roughness R_a, μm
NP5	0.17	1104	7.85	0.924
NP10	0.15	1095	8	1.38
NP15	0.18	1080	16.86	1.24
NP20	0.20	1003	19.71	1.55
SS5	0.15	1819	24.58	0.894
SS10	0.11	1712	11.85	1.43
SS15	0.19	1896	28.99	1.36
SS20	0.13	1888	30.66	1.44

REFERENCES

1. Ma, Y., et al., *J. Mater. Process. Technol.,* 2007, vol. 182, p. 58.
2. Raj, V.M. and Mubarak, A., *J. Mater. Process. Technol.,* 2009, vol. 209, p. 5341.
3. Erdemir, A., in *Handbook of Deposition Technologies for Films and Coatings,* Martin, P.M., Ed., New York: Elsevier, 2010.
4. Guo, H.M., *Thin Solid Films,* 2006, vol. 500, p. 186.
5. Cakmak, E., et al., *Surf. Coat. Technol.,* 2010, vol. 204, p. 1305.
6. Jovović, J., et al., *J. Quant. Spectrosc. Radiat. Transfer,* 2012, vol. 113, p. 1928.
7. Guo, H., et al., *Trans. Nonferrous Met. Soc. China,* 2012, vol. 22, p. 1786.
8. Aliofkhazraei, M., Rouhaghdam, A.S., and Shahrabi, T., *Surf. Coat. Technol.,* 2010, vol. 205, p. 41.
9. Durdu, S. and Usta, M., *Ceram. Int.,* 2014, vol. 40, p. 3627.
10. Li, X. and Luan, B.L., *Mater. Lett.,* 2012, vol. 86, p. 88.
11. Aliofkhazraei, M. and Rouhaghdam, A.S., *Appl. Surf. Sci.,* 2012, vol. 258, p. 2093.
12. Al Bosta, M.M.S. and Ma, K.-J., *Appl. Surf. Sci.,* 2014, vol. 308, p. 121.
13. Matykina, E., et al., *Appl. Surf. Sci.,* 2008, vol. 255, p. 2830.
14. Lee, K.M., et al., *Surf. Coat. Technol.,* 2011, vol. 205, p. 3779.
15. Yue Yangy, H.W., *Mater. Sci. Technol.,* 2010, vol. 26, p. 865.
16. Gnedenkov, S.V., et al., *Vacuum,* 2015, vol. 120, pp. 107–114.
17. Sarbishei, S., Faghihi Sani, M.A., and Mohammadi, M.R., *Vacuum,* 2014, vol. 108, p. 12.
18. Wang, Y.Q., Zheng, M.Y., and Wu, K., *Mater. Lett.,* 2005, vol. 59, p. 1727.
19. Barchiche, C.E., et al., *Electrochim. Acta,* 2007, vol. 53, p. 417.
20. Liang, J., et al., *Electrochim. Acta,* 2009, vol. 54, p. 3842.
21. Gnedenkov, S.V., et al., *Surf. Coat. Technol.,* 2013, vol. 232, p. 240.
22. Ma, C., et al., *Tribol. Int.,* 2012, vol. 47, p. 62.
23. Correa, E., et al., *Wear,* 2013, vol. 305, p. 115.
24. Srinivasan, P.B., et al., *Appl. Surf. Sci.,* 2010, vol. 256, p. 3265.
25. Li, X., Liu, X., and Luan, B.L., *Appl. Surf. Sci.,* 2011, vol. 257, p. 9135.
26. Cui, S., et al., *Surf. Coat. Technol.,* 2007, vol. 201, p. 5306.
27. Tacikowski, M., et al., *J. Magnesium Alloys,* 2014, vol. 2, p. 265.